Journal of Marine Systems 159 (2016) 33–40

Contents lists available at ScienceDirect

Journal of Marine Systems

journal homepage: www.elsevier.com/locate/jmarsys

Observed strong currents under global tropical cyclones

Yu-Chia Chang [a], Ruo-Shan Tseng [b,*], Peter C. Chu [c], Jau-Ming Chen [d], Luca R. Centurioni [e]

[a] Department of Marine Biotechnology and Resources, National Sun Yat-sen University, Kaohsiung 80424, Taiwan
[b] Department of Oceanography, National Sun Yat-sen University, Kaohsiung 80424, Taiwan
[c] Naval Ocean Analysis and Prediction Laboratory, Naval Postgraduate School, Monterey, CA 93943, USA
[d] Institute of Maritime Information and Technology, National Kaohsiung Marine University, Kaohsiung 80543, Taiwan
[e] Scripps Institution of Oceanography, La Jolla, CA 92093-0213, USA

ARTICLE INFO

Article history:
Received 24 October 2015
Received in revised form 2 March 2016
Accepted 3 March 2016
Available online 8 March 2016

Keywords:
SVP drifter
Tropical cyclones
Translation speed
Ocean currents
Northern Hemisphere
Southern Hemisphere

ABSTRACT

Global data from drifters of the Surface Velocity Program (Niiler, 2001) and tropical cyclones (TCs) from the Joint Typhoon Warning Center and National Hurricane Center were analyzed to demonstrate strong ocean currents and their characteristics under various storm intensities in the Northern Hemisphere (NH) and in the Southern Hemisphere (SH). Mean TC's translation speed (U_h) is faster in the NH (~4.7 m s^{-1}) than in the SH (~4.0 m s^{-1}), owing to the fact that TCs are more intense in the NH than in the SH. The rightward (leftward) bias of ocean mixed-layer (OML) velocity occurs in the NH (SH). As a result of this slower U_h and thus a smaller Froude number in the SH, the flow patterns in the SH under the same intensity levels of TCs are more symmetric relative to the TC center and the OML velocities are stronger. This study provides the first characterization of the near-surface OML velocity response to all recorded TCs in the SH from direct velocity measurements.

1. Introduction

Ocean mixed-layer (OML) velocities under a moving tropical cyclone (TC) are mainly determined by the wind stress, the storm's translation speed (U_h), the storm's size (the radius of the maximum tangential velocity of the storm, R), and the OML depth (Price, 1981, 1983; Price et al., 1994; Chang et al., 2013, 2014). In-situ observations of current velocities under TCs were rare and often with a fortuitous nature. The platforms of measuring upper-ocean response to TCs in the past can be mainly divided into two types. The first one is by deploying airborne drifting or profiling instruments, such as expendable current profilers (AXCPs), electromagnetic-autonomous profiling explorer (EM-APEX) floats, surface drifters or Lagrangian floats (Price et al., 1994; D'Asaro et al., 2007; Sanford et al., 2011) ahead of a target hurricane. The second method of observing ocean current response to TCs is by using data collected from current meter mooring or shore-based high frequency radar during the passage of hurricanes (Brooks, 1983; Teague et al., 2007; Jaimes and Shay, 2009; Black and Dickey, 2008). Both methods provide direct measurements of ocean currents and thermal structure in response to a moving TC, and the various factors of the ocean thermal structure which affect this response can be discussed separately.

Among the above-mentioned instruments to detect the typhoon–ocean interaction, surface drifter has the advantage of being able to operate under high sea states with a relatively low cost and long durability. To date, the Global Drifter Program has been maintaining a global 5 × 5 degree array of 1250 satellite-tracked surface drifting buoys to meet the need for an accurate and globally dense set of in-situ observations of mixed layer currents. The drifter dataset can be incorporated with the historical typhoon database to obtain the typhoon-induced near-surface current in different years and at various oceans. We have studied the strong surface flow in the North Pacific and Taiwan Strait under the influence of several typhoons using drifters (Chang et al., 2010, 2014). Chang et al. (2013), on the other hand, have compiled from all drifter data in the Northwest Pacific over a long period of time (1985–2009) and obtained a statistical result of spatial distribution of surface currents relative to the TC's center, and their result compares favorably with the classical theory of Geisler (1970) and the modeling results of Price (1983).

TC climatology of the Southern Hemisphere (SH) indicates that somewhat different characteristics exist between the TCs in the Northern Hemisphere (NH) and SH in terms of the storm's translation speed and intensity (Dowdy et al., 2012). On the other hand, previous measurements of ocean current response in the OML to the TCs were mostly conducted in the oceans of the NH. Questions arise: Are these results valid for the Southern Hemisphere (SH)? If not, what are the characteristics of observed ocean current response under TCs with all intensity-levels in the SH? What does an average hurricane response look like in the SH? The goal of this study is to characterize the observed near-surface currents under TCs with all intensity-levels for the global

* Corresponding author.
E-mail address: rstseng@mail.nsysu.edu.tw (R.-S. Tseng).

http://dx.doi.org/10.1016/j.jmarsys.2016.03.001
0924-7963/

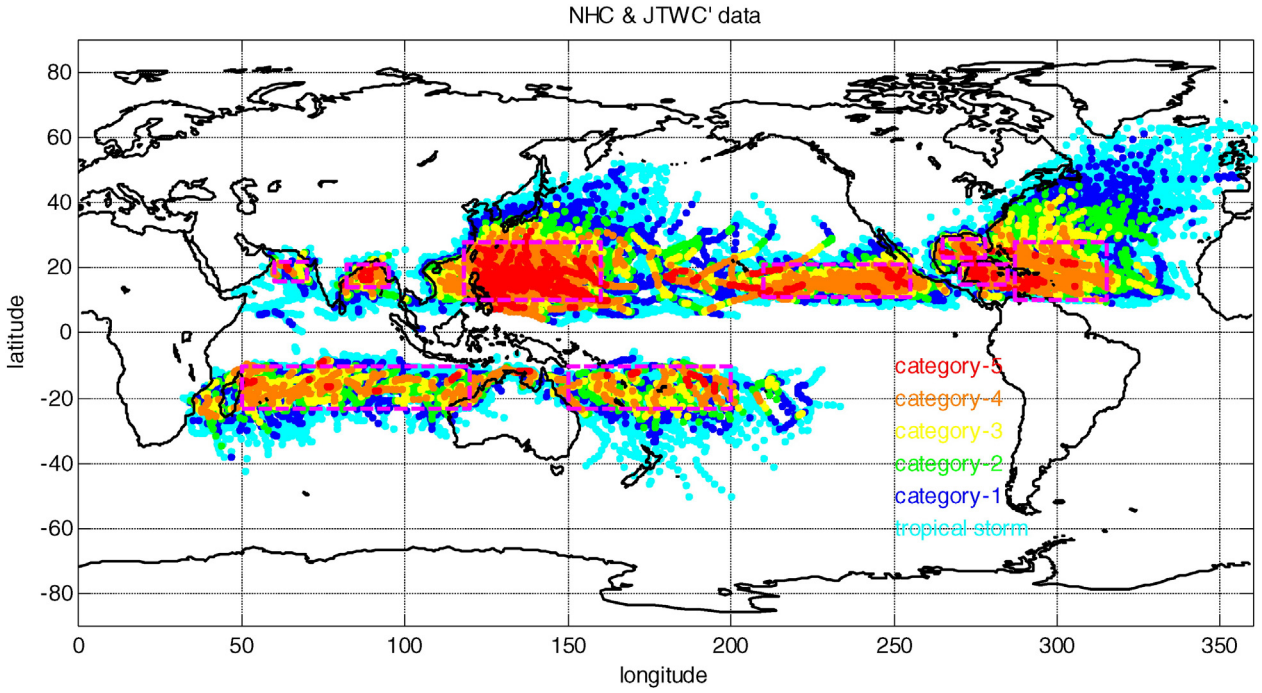

Fig. 1. Global TC's locations color coded with Saffir–Simpson Scale from JTWC (1979–2013) and NHC (1979–2013). The magenta boxes are the main TC development regions (see text).

ocean. Data analysis methods for global drifters under the influence of TCs similar to Chang et al. (2013) were used in this study. Data and method will be described in Section 2. Storm characteristics such as the mean and standard deviation of translation speed and moving direction for the NH and SH, deduced from long-term storm's best track data, will be presented in Section 3. The observed OML current velocities under TCs and their spatial distribution relative to the storm center will be described in Section 4, followed by a discussion and concluding remarks.

2. Data and method

Global TC data with 6-hour temporal resolution were acquired from the Joint Typhoon Warning Center (JTWC) best track dataset and the National Hurricane Center (NHC) best track dataset. JTWC provides the TCs best track data in the SH, North Indian Ocean, and Northwest Pacific Ocean. NHC provides TCs best track data in the Northeast Pacific Ocean and North Atlantic Ocean.

Direct velocity measurements in the OML are obtained with satellite-tracked drifters drogued at a nominal depth of 15 m. Drifter data were acquired from an enhanced version of the global drifter dataset maintained at Atlantic Oceanographic and Meteorological Laboratory (AOML; available online at http://www.aoml.noaa.gov/phod/dac/dacdata.html) (Niiler, 2001). Drifter positions are determined every few hours, depending on latitudes, by Doppler ranging with the Argos satellite system. Time series of irregular drifter positions are interpolated to a 6-hr interval through Kriging. The estimated accuracy of the velocity measurements in a 10 m s^{-1} wind is 10^{-2} m s^{-1} (Niiler et al., 1995). In addition to the measurements from drogued drifters, velocity data from undrogued drifters are recovered with the calibration procedure described by Pazan and Niiler (2001) and used in this study.

Atmospheric features are diagnosed from the NCEP/NCAR Reanalysis monthly data. NOAA Earth System Research Laboratory (ESRL) (http://www.esrl.noaa.gov/psd/data/gridded/data.ncep.reanalysis.pressure.html) provides the NCEP/NCAR Reanalysis wind data (2.5° × 2.5° grids) in the global atmosphere at 17 pressure levels (1000, 925, 850, 700, 600, 500, 400, 300, 250, 200, 150, 100, 70, 50, 30, 20, and 10 mb). The ERSST and reanalysis wind data are jointly used to examine large-scale regulatory processes of the ocean–atmosphere system for TC activity in the global domain.

NOAA National Oceanographic Data Center (NODC) provides the statistical fields of observed profile data interpolated to standard depth levels (0, 10, 20, 30, 50, 75, 100, 125, 150, 200, 250, 300, 400, 500, 600, 700, 800, 900, 1000, 1100, 1200, 1300, 1400, 1500 m) on

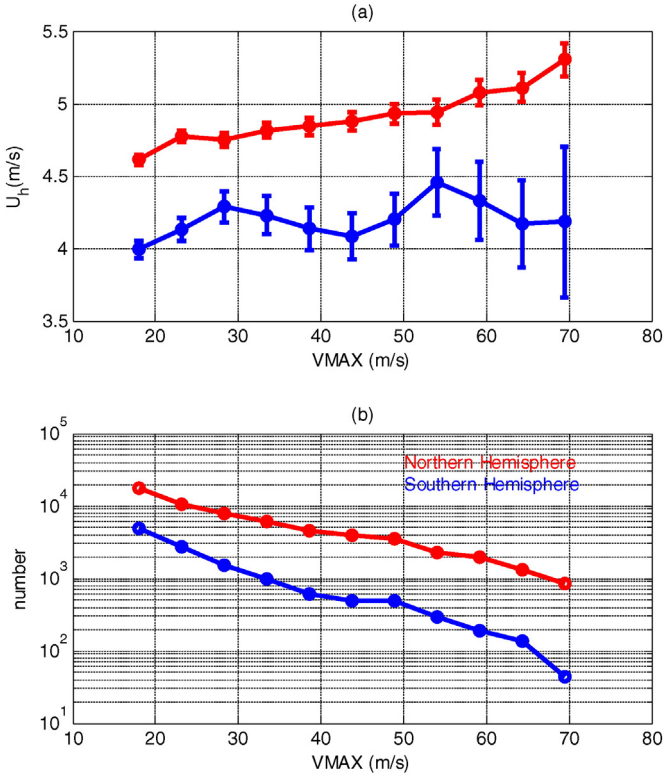

Fig. 2. Dependence of (a) translation speed (U_h), and (b) pair number on maximum sustained wind speed (*VMAX*) with the 95% confidence intervals in (a).

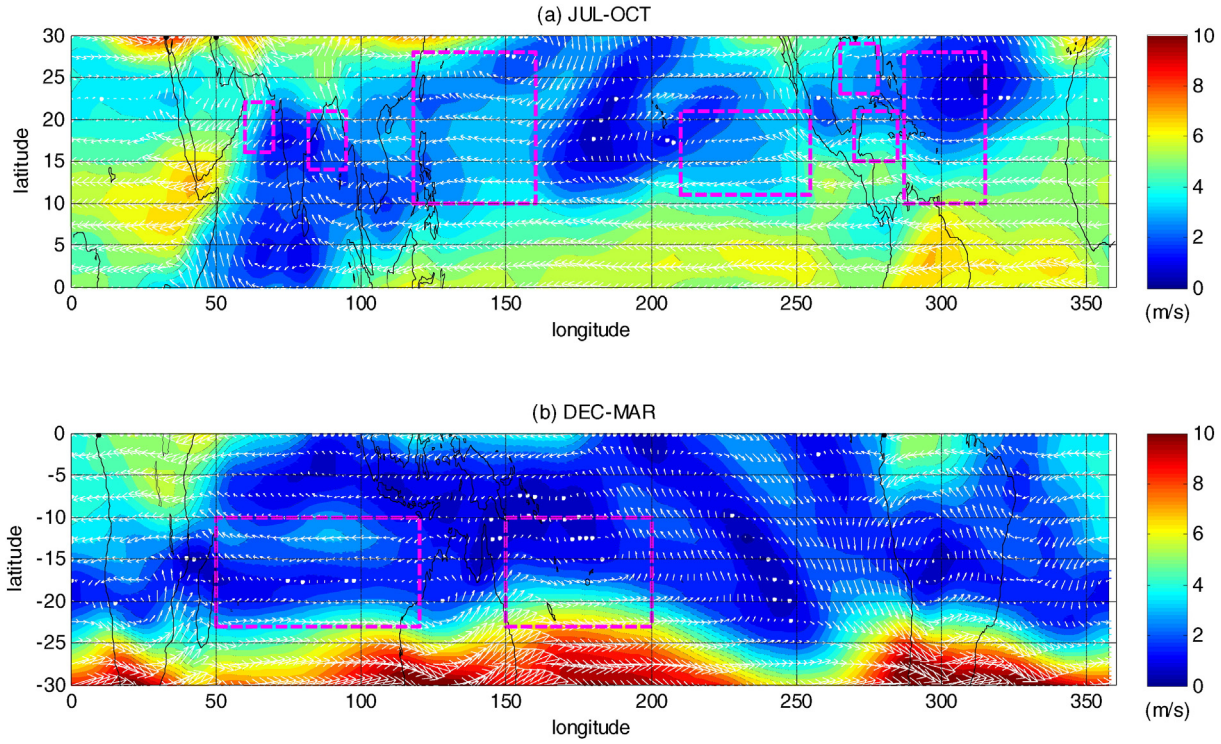

Fig. 3. Mean wind vectors (below 300 mb; from Earth's surface to a height of about 12 km) from the NCEP/NCAR Reanalysis wind data (1979–2013) during (a) July–October and (b) December–March. The magenta boxes are the main tropical cyclone development region. (For interpretation of the references to color in this figure legend, the reader is referred to the web version of this article.)

1° × 1° grids (World Ocean ATLAS 2009; https://www.nodc.noaa.gov/) in the global ocean. The statistical field is a set of objectively analyzed oceanographic fields of in situ temperature, salinity for monthly compositing periods.

3. Storm's translation speeds in the Northern and Southern Hemispheres

Fig. 1 shows all storms' locations from JTWC (1979–2013) and NHC (1979–2013). The locations of TCs are presented in Fig. 1 with various intensities based on the Saffir–Simpson Scale, such as category-5, -4, -3, -2, -1, tropical storm (TS), and tropical depression (TD). TCs occur most frequently in the North Pacific, followed by the Indian Ocean, North Atlantic, and Southwest Pacific. This result is consistent with previous studies (e.g., Menkes et al., 2012, Lloyd and Vecchi, 2011). Note that the Northwest Pacific is the region which has the most intense TCs among all basins, followed by the North Atlantic. The evolution of TC intensity depends mainly on three factors: its initial intensity, dynamic and thermodynamic state of the atmosphere, and heat exchange with the upper ocean (Emanuel, 1988, 1999, 2005; Lin et al., 2013; Mei et al., 2015). Fig. 2 shows TC translation speed (U_h) as a function of maximum sustained wind speed (*VMAX*) with a 95% confidence

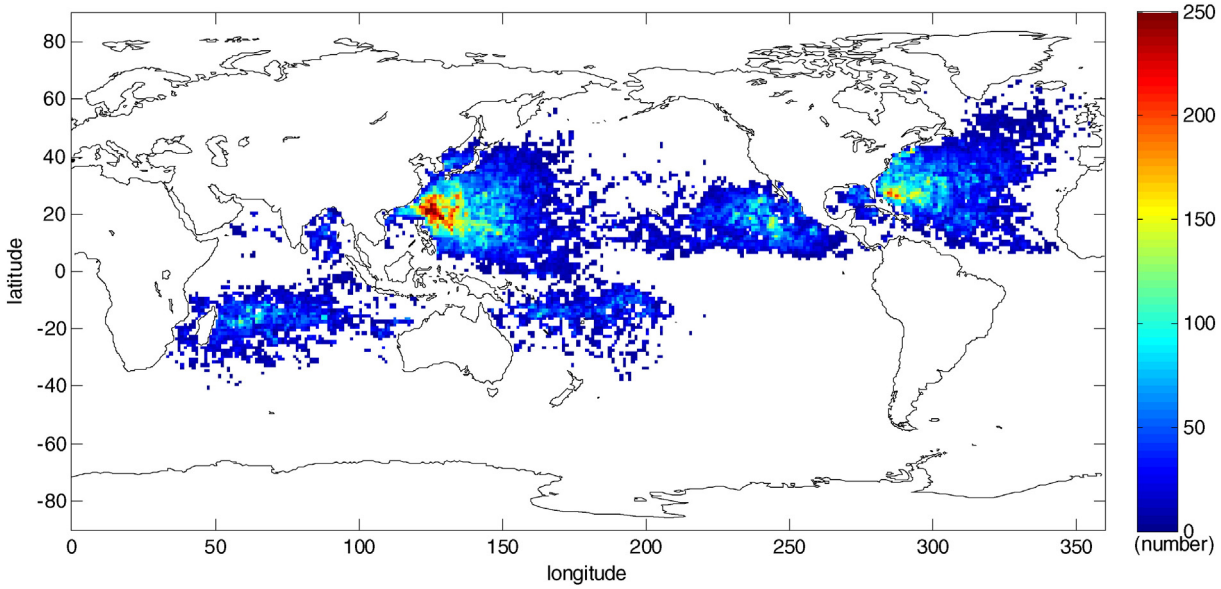

Fig. 4. The number of drifter data (294,693 data points) within 1° × 1°grid under all storms (distance < 800 km) during 1979–2012.

interval. The mean of translation speed is calculated for each bin of wind speed. Mei et al. (2012) found a net increase of U_h with TC category from global TC data. In this study, the mean U_h also correlates closely with the maximum sustained wind speed (The correlation coefficient R = 0.96 in the NH and R = 0.94 in the SH). Mean translation speeds range between 4.6 and 5.3 m s^{-1}, and between 4.0 and 4.5 m s^{-1} in the NH and SH, respectively (Fig. 2). In this study, we find that mean U_h for all recorded TCs in the SH (~4.0 m s^{-1}) is slower than that in the NH (~4.7 m s^{-1}). This is due to the fact that TCs in the SH are mostly not very strong, as a result the mean U_h is smaller than that in the NH. TCs appear frequently during July–October (December–March) in the NH (SH). Fig. 3 shows the vertically averaged wind vectors (below 300 mb; from Earth's surface to a height of about 12 km), derived from NCEP data between 1979 and 2013, in the main TC development region in the summer of NH (Fig. 3a, during July–October) and SH (Fig. 3b, during December–March). The Northeast Pacific is the region which has the strongest mean wind speed, followed by the North Atlantic, South Indian Ocean, North Indian Ocean, Northwest Pacific and Southwest Pacific. The mean NCEP wind speed is about 11.1 m s^{-1} in the NH and about 8.3 m s^{-1} in the SH. It should be noted that the movement of a TC is not only influenced by steering flow and beta drift effect, but also by other factors such as cyclone structure. The path of a storm depends primarily upon the steering flow by the environmental winds in which it is embedded.

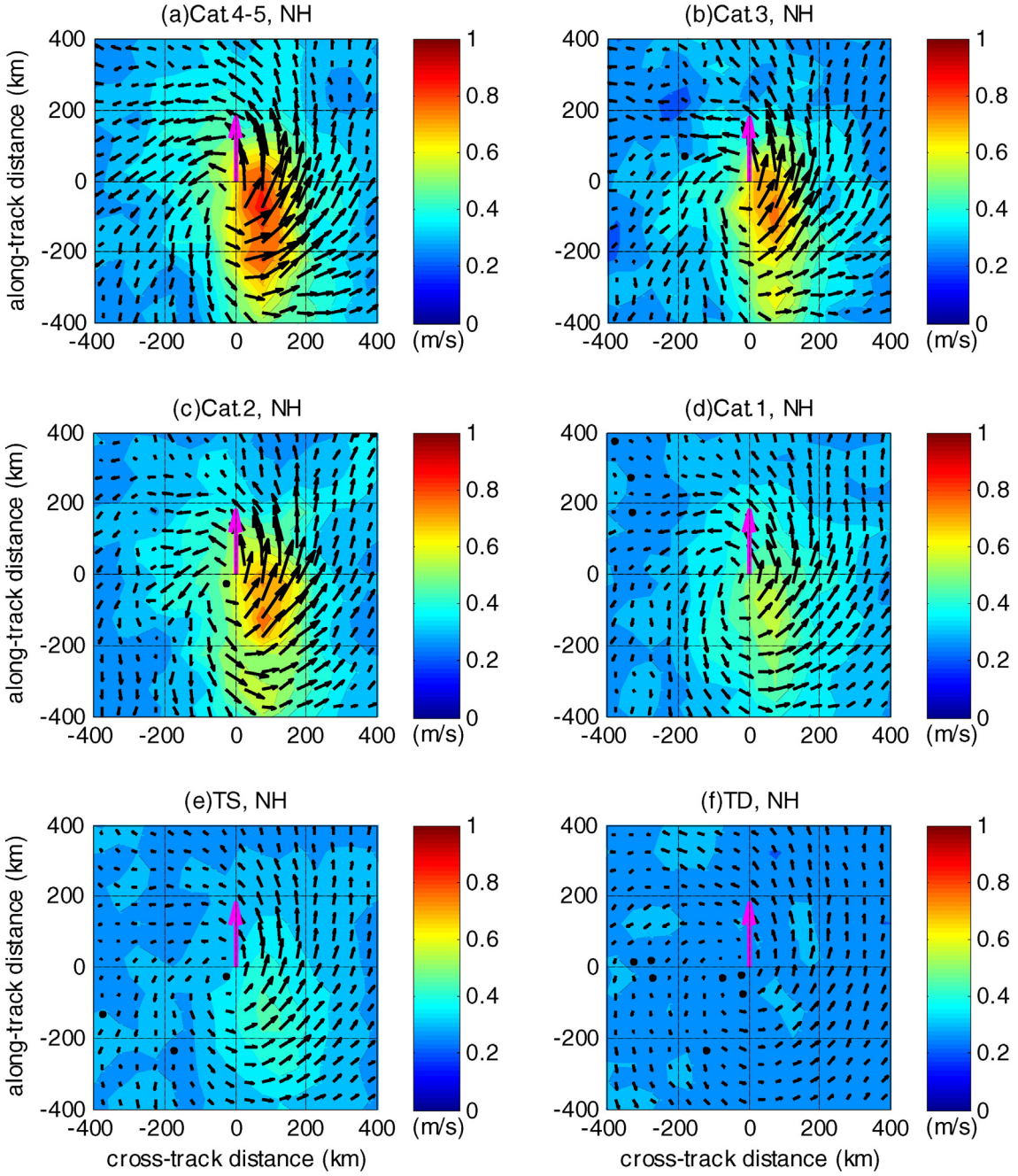

Fig. 5. Mean current vectors (m s^{-1}) under (a) category-4 and -5, (b) category-3, (c) category-2, (d) category-1 TCs, (e) tropical storm and (f) tropical depression in the Northern Hemisphere. Magenta arrows indicate storm movement in the positive along-track direction. (For interpretation of the references to color in this figure legend, the reader is referred to the web version of this article.)

4. Observed OML currents under tropical cyclones in the Northern and Southern Hemispheres

Generally, TCs move west-to-northwestward in the NH and southwestward in the SH. In order to obtain statistical characteristics of the spatial distribution for observed current vectors relative to the TC center, the Cartesian coordinate is rotated into the storm-coordinate system with the unit vectors in the along-track and cross-track directions (Price, 1981; Price, 1983; Chang et al., 2013). The relative locations and distances (D) between a storm center and a nearby drifter are estimated at the same UTC time. Fig. 4 shows the number of drifter data within each cell of 1° × 1° during 1979–2012 under all storms, with the requirement of $D < 800$ km. Note that of the total global number of drifter data (294,693), the Northwest Pacific and North Atlantic have the most data points, followed by the Northeast Pacific, South Indian, and South Pacific. There are relatively less number of data in the North Indian. Table 2 lists the number of 6-hourly observations of drifters in the NH and SH, respectively. The number of drifter data points in the NH is about four times as many as in the SH. Current vectors derived from drifters were processed by the ensemble average method (Centurioni and Niiler, 2003; Centurioni et al., 2004) to show the mean and standard deviation of velocities for each bin (40 km × 40 km). Figs. 5 and 6 show spatial distribution of current vectors under various TC intensity levels in the NH and SH, respectively. Note that the TCs move in the positive (negative) along-track direction in the NH (SH), as indicated by the magenta arrows in Figs. 5 and 6. In the NH (SH), the OML currents under TCs rotate counterclockwise (clockwise). Strong rightward (leftward) biased currents in the OML can be

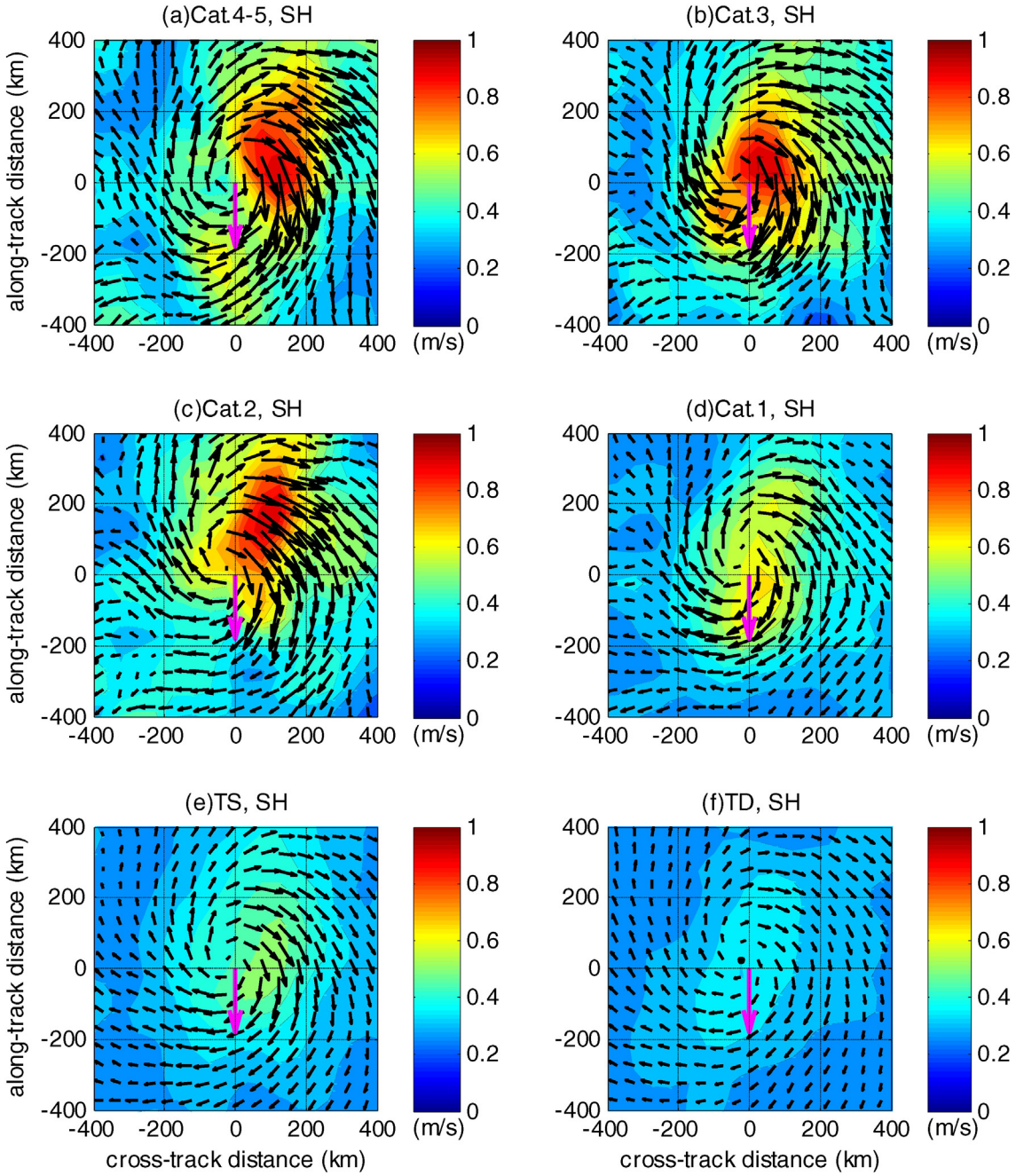

Fig. 6. Mean current vectors (m s^{-1}) under (a) category-4 and -5, (b) category-3, (c) category-2, (d) category-1 TCs, (e) tropical storm and (f) tropical depression in the Southern Hemisphere. Magenta arrows indicate storm movement in the negative along-track direction. (For interpretation of the references to color in this figure legend, the reader is referred to the web version of this article.)

Table 1
Mean storm's translation speeds (U_h), ocean mixed-layer depths (h), the phase speed of the first baroclinic mode (c_1), the Froude number (F_r) in the Northern Hemisphere (NH), Southern Hemisphere (SH), and different basins.

Region	NH	North Atlantic	Northwest Pacific	Northeast Pacific	North Indian	SH	South Pacific	South Indian
U_h (m s^{-1})	4.7	4.9	4.8	4.6	3.8	4.0	4.1	4.0
h (m)	40	43	42	34	37	38	37	39
c_1 (m s^{-1})	2.5	2.2	2.8	2.1	2.9	2.7	2.8	2.6
Fr	1.9	2.2	1.7	2.2	1.3	1.5	1.5	1.5

identified under all storm intensities in the NH (SH). This phenomenon is more pronounced for more intense TCs, and is less evident as the intensity of TCs decreases. The current field under TCs of various intensity levels compiled from all oceans in the NH (Fig. 5) is very similar to our previous results in the Northwest Pacific (Chang et al., 2013). On the other hand, Fig. 6 provides the first characterization of the near-surface velocity response in the SH to all recorded TCs in terms of a relatively long time series of direct velocity measurements. Maximum standard deviations of speeds under the category-4 and -5 TCs (TD) in the NH and SH are about 0.6 (0.3) and 0.4 (0.2) m s^{-1}, respectively. These standard deviations of speeds are mainly caused by the effects of OML depth, storm's translation speeds, storm's size, local background flow, and Stokes drift (Price, 1983; Price et al., 1994; Chang et al., 2013, 2014). The 6-hourly OML depth, storm's U_h and storm's size vary in time and space. The local background flow (or eddies of various length scales) affects the observed current structure and velocity (Gill, 1984) as well as the ocean mixed-layer depth (e.g. Jullien et al., 2014). The drifters are drogued at the 15-m depth, which is still in a region of significant Stokes drift influence. The largest Stokes drift is about 0.5 m s^{-1} at the ocean surface under a category-4 TC on the right-hand side of the storm track (Sullivan et al., 2012). The OML cross-track currents in the storm's wake are mainly due to the wind stress with the maximum current speed to the right of the storm track at $y = 2R$, where R is the radius of the maximum tangential velocity of the storm (Brooks, 1983). For all TC intensity levels, the distance between the velocity maximum and storm center is approximately 100 km (~$2R$, mean $R = 47$ km from Hsu and Yana (1998)) in the NH and SH (Figs. 5 and 6). However, it should be noted that the location of the strongest currents is mainly determined by the translation speed of the storm, and not always $2R$ (~100 km) from theory (D'Asaro et al., 2014). The left-to-right asymmetry in velocity amplitude depends mainly on the resonant coupling between clockwise-rotating (counterclockwise-rotating) wind stress and near-inertial currents on the right (left) side of a storm in the NH (SH), where the strongest wind stress occurs. The asymmetry of the observed velocity fields also agrees with the previous studies (Price, 1981; Price et al., 1994; Chu et al., 2000; Chang et al., 2013). Our new findings are more symmetric current field in the SH than in the NH, and stronger maximum velocity occurs in the SH than in the NH (Figs. 5 and 6).

An important linear theory (Geisler, 1970) indicates that inertial-gravity waves are the dominant feature of the upper ocean if the translation speed of the storm exceeds the phase speed of the first baroclinic mode (c_1). If the TC is moving at a speed (U_h) more than a few times the phase speed of the first baroclinic mode (i.e., the Froude number, $F_r = U_h/c_1 \gg 1$), the currents in the wake become more near inertial after the first half inertial period (Chang and Anthes, 1978; Chang, 1985; Ginis and Sutyrin, 1995). If the translation speeds are closer to the baroclinic long wave speed ($F_r = U_h/c_1 \sim 1$), the wake becomes a perturbation on a smooth pattern of upwelling. If the translation speeds are below c_1 ($F_r = U_h/c_1 < 1$), the oceanic response is a barotropic, geostrophical gyre with upwelling in the storm's center. To evaluate the near-inertial velocity response over the NH and SH oceans, c_1 can be estimated from a simple two-layer approach (Jaimes and Shay, 2009), i.e., from the density changes and layer thicknesses of the OML and the thermocline. In the coastal ocean, c_1 ranges between 0.1 and 0.5 m s^{-1}, whereas in the deep ocean, phase speeds range between 1 and 3 m s^{-1} (Steele et al., 2009). The wave phase speeds of the first baroclinic mode during summer are estimated from the NODC temperature and density profiles in the Northwest Pacific (~2.8 m s^{-1}), in the North Atlantic (~2.2 m s^{-1}), in the Northeast Pacific (~2.1 m s^{-1}), in North Indian Ocean (~2.9 m s^{-1}), in the Southwest Pacific (~2.8 m s^{-1}), and in South Indian Ocean (~2.6 m s^{-1}), respectively (Jaimes and Shay, 2009; Chang et al., 2013). In the TCs-rich zone, c_1 ranges between 2 and 3 m s^{-1}. Table 1 lists the U_h, c_1, and F_r for all basins. Storm's U_h in the NH (4.7 m s^{-1}) is about 18% greater than that in the SH (4.0 m s^{-1}). Values of estimated F_r are ~2.2 in the North Atlantic, ~2.2 in the Northeast Pacific, ~1.7 in the Northwest Pacific, ~1.3 in North Indian Ocean, ~1.7 in the Southwest Pacific, and ~1.5 in South Indian Ocean. Storm's F_r in the NH (1.9) is about 27% greater than that in the SH (1.5). Therefore, it is reasonable to infer that the velocity fields in the SH (NH) have weakly (strongly) left-to-right asymmetric distributions, as evidenced in Figs. 5 and 6, based on the Geisler's (1970).

On the other hand, the wind-driven velocity in the OML under a moving TC can be represented by a horizontal velocity scale U_s (Price, 1983; Price et al., 1994), i.e.

$$U_s = \frac{\tau R}{h U_h} \tag{1}$$

where τ is the surface wind stress, and h is the OML depth. It should be noted that Eq. (1) is nonlinear. Fig. 7(a) and (b) shows the OML depths in the summer of NH and SH, respectively, estimated from NODC temperature profiles with an optimal temperature difference of 0.2 °C (de Boyer Monte'gut et al., 2004). The mean OML depths of main development region during summer are ~43 m in the North Atlantic, ~34 m in the Northeast Pacific, ~42 m in the Northwest Pacific, ~37 m in North Indian Ocean, ~37 m in the Southwest Pacific, and ~39 m in South Indian Ocean (Table 1). Overall, the mean OML depths of main development region during summer in the NH (~40 m) and SH (~38 m) are similar, as shown in Fig. 7. The estimated OML depths in this study are close to those in the earlier study (de Boyer Monte'gut et al., 2004). The TCs act to deepen the climatological OML depth. According to a previous study (Fu et al., 2014), the averaged OML depth changes under TC influence are about 20–30 m. There are rarely direct surface wind data available in the NH and in the SH. The wind data in TCs from operational aircraft reconnaissance are exceptional. From available data, mean R is

Table 2
Numbers of data points under category-4 and -5, category-3, category-2, category-1 TCs, tropical storm and tropical depression in the Northern Hemisphere and Southern Hemisphere.

Ocean basin	Northern Hemisphere	Southern Hemisphere
Category-4 &-5	12,951	3979
Category-3	10,392	4119
Category-2	14,484	4432
Category-1	30,552	8531
TS	83,614	18,790
TD	83,719	19,130
Total	235,712	58,981

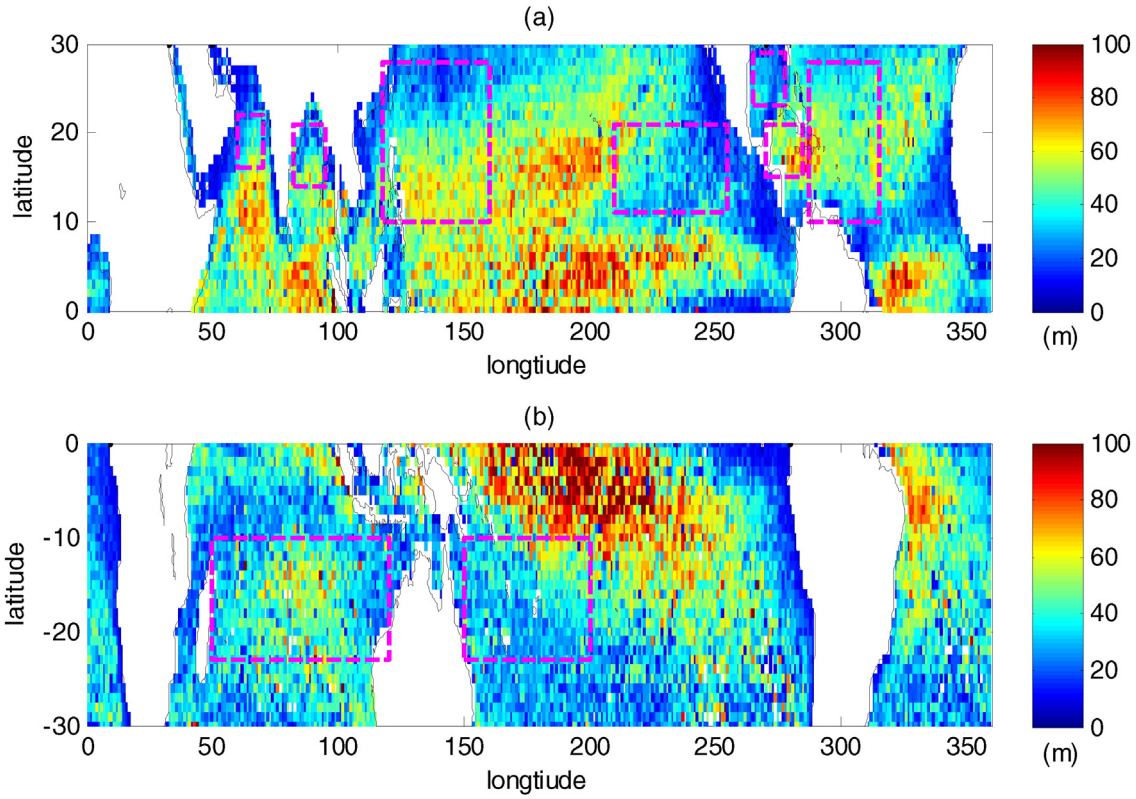

Fig. 7. Ocean mixed-layer (OML) depths estimated from NODC temperature profiles, with an optimal temperature difference of 0.2 °C (de Boyer Monte'gut et al., 2004) (a) in the Northern Hemisphere (July–October) and (b) the Southern Hemisphere (December–March), respectively.

about 49.7 km in the NH and about 48.6 km in the SH. They are very similar to mean R of 47 km in the earlier study (Hsu and Yana, 1998). The maximum velocity from drifter measurements in the SH (Fig. 6) is greater than that in the NH (Fig. 5). Based on Eq. (1) and the estimated mean values of R (49.7 and 48.6 km), h (40 and 38 m), and U_h (4.7 and 4.0 m s^{-1}) in the NH and SH, it implies that TC's translation speed U_h is principally responsible for the North/South difference in currents because the hemispheric difference in U_h (~15%) is more significant than the other two factors (~2% and ~5%).

5. Summary

Flow patterns of strong currents under various TC intensity levels in the NH and SH are illustrated comprehensively from large amounts of drifter data over a long period of time. The rightward (leftward) bias of OML velocity occurs in the NH (SH). Mean translation speed of all TCs is slower in the SH than in the NH, but the phase speed of the first baroclinic mode estimated from NODC mean temperature and salinity profiles is approximately equal for the SH and NH. As a result, the flow patterns are more symmetric and OML velocities are stronger in the SH than in the NH. To the best of our knowledge, the present study successfully provides a first statistical, spatial characterization of near-surface velocity response to all recorded TCs in the SH, which is in agreement with the theoretical prediction. Overall, our results show what an average hurricane response looks like, nicely complementing other efforts that highlight the effect of the initial ocean state.

Acknowledgements

This research was completed with grants from the Ministry of Science and Technology of Taiwan, Republic of China (MOST 102-2611-M-110-010-MY3). Peter C. Chu was supported by the Naval Oceanographic Office. SVP drifter data (NOAA/AOML; http://www.aoml.noaa.gov/phod/dac/dacdata.html), storm data (JTWC&NHC; http://www.usno.navy.mil/NOOC/nmfc-ph/RSS/jtwc/best_tracks/; http://www.nhc.noaa.gov/data/), hydrologic data (NODC; https://www.nodc.noaa.gov/), and NCEP wind data (http://www.esrl.noaa.gov/psd/data/gridded/data.ncep.reanalysis.pressure.html) in this study are available for free.

References

Black, W.J., Dickey, T.D., 2008. Observations and analyses of upper ocean responses to tropical storm and hurricanes in the vicinity of Bermuda. J. Geophys. Res. 113, C08009. http://dx.doi.org/10.1029/2007JC004358.

Brooks, D.A., 1983. The wake of Hurricane Allen in the western gulf of Mexico. J. Phys. Oceanogr. 13, 117–129.

Centurioni, L.R., Niiler, P.P., 2003. On the surface currents of the Caribbean Sea. Geophys. Res. Lett. 30, 1279. http://dx.doi.org/10.1029/2002GL016231.

Centurioni, L.R., Niiler, P.P., Lee, D.K., 2004. Observations of inflow of Philippine Sea surface Water into the South China Sea through the Luzon Strait. J. Phys. Oceanogr. 34, 113–121.

Chang, S.W., 1985. Deep ocean response to hurricanes as revealed by an ocean model with free surface. Part I: axisymmetric case. J. Phys. Oceanogr. 15, 1847–1858.

Chang, S.W., Anthes, R.A., 1978. Numerical simulations of the ocean's nonlinear baroclinic response to translating hurricanes. J. Phys. Oceanogr. 8, 468–480.

Chang, Y.-C., Tseng, R.-S., Centurioni, L.R., 2010. Typhoon-induced strong surface flows in the Taiwan Strait and Pacific. J. Oceanogr. 66, 175–182.

Chang, Y.-C., Chen, G.-Y., Tseng, R.-S., Centurioni, L.R., Chu, P.C., 2013. Observed near-surface flows under all tropical cyclone intensity levels using drifters in the Northwestern Pacific. J. Geophys. Res. 118, 2367–2377.

Chang, Y.-C., Chu, P.C., Tseng, R.-S., Centurioni, L.R., 2014. Observed near-surface currents under four super typhoons. J. Mar. Syst. 139, 311–319.

Chu, P.C., Veneziano, J.M., Fan, C.W., 2000. Response of the South China Sea to tropical cyclone Ernie 1996. J. Geophys. Res. 105, 13991–14009.

D'Asaro, E.A., Black, P.G., Centurioni, L.R., Chang, Y.-T., Chen, S.S., Foster, R.C., Graber, H.C., Harr, P., Hormann, V., Lien, R.-C., Lin, I.-I., Sanford, T.B., Tang, T.-Y., Wu, C.-C., 2014. Impact of typhoons on the ocean in the Pacific: ITOP. Bull. Am. Meteorol. Soc. 95, 1405–1418.

D'Asaro, E.A., Sanford, T.B., Niiler, P.P., Terrill, E.J., 2007. Cold wake of Hurricane Frances. Geophys. Res. Lett. 34, L15609. http://dx.doi.org/10.1029/2007GL030160.

de Boyer Monte'gut, C., Madec, G., Fischer, A.S., Lazar, A., Iudicone, D., 2004. Mixed layer depth over the global ocean: an examination of profile data and a profile-based climatology. J. Geophys. Res. 109, C12003. http://dx.doi.org/10.1029/2004JC002378.

Dowdy, A.J., Qi, L., Jones, D., 2012. Tropical cyclone climatology of the South Pacific Ocean and its relationship to El Nino-Southern Oscillation. J. Clim. 25, 6108–6122.
Emanuel, K.A., 1988. The maximum intensity of hurricanes. J. Atmos. Sci. 45, 1143–1155.
Emanuel, K.A., 1999. Thermodynamic control of hurricane intensity. Nature 401, 665–669.
Emanuel, K.A., 2005. Increasing destructiveness of tropical cyclones over the past 30 years. Nature 403, 686–688.
Fu, H.-L., Wang, X.-D., Chu, P.C., Zhang, X.-F., Han, G.-J., Li, W., 2014. Tropical cyclone footprint in the ocean mixed layer observed by Argo in the Northwest Pacific. J. Geophys. Res. 119 (11), 8078–8092.
Geisler, J.E., 1970. Linear theory of the response of a two-layer ocean to a moving hurricane. Geophys. Fluid Dyn. 1, 249–272.
Gill, A.E., 1984. On the behavior of internal waves in the wake of storms. J. Phys. Oceanogr. 14, 1129–1151.
Ginis, I., Sutyrin, G., 1995. Hurricane-generated depth-averaged currents and sea surface elevation. J. Phys. Oceanogr. 25, 1218–1242.
Hsu, S.A., Yana, Z., 1998. A note on the radius of maximum winds for hurricanes. J. Coast. Res. 12, 667–668.
Jaimes, B., Shay, L.K., 2009. Mixed layer cooling in mesoscale oceanic eddies during hurricanes Katrina and Rita. Mon. Weather Rev. 137, 4188–4207.
Jullien, S., Marchesiello, P., Menkes, C.E., Lefevre, J., Jourfain, N.C., Samson, G., Lengaigne, M., 2014. Ocean feedback to tropical cyclones: climatology and processes. Clim. Dyn. 43 (9), 2831–2854.
Lin, I.-I., Black, P., Price, J.F., Yang, C.-Y., Chen, S.S., Lien, C.-C., Harr, P., Chi, N.-H., Wu, C.-C., D'Asaro, E.A., 2013. An ocean coupling potential intensity index for tropical cyclones. Geophys. Res. Lett. 40, 1878–1882. http://dx.doi.org/10.1002/grl.50091.
Lloyd, I.D., Vecchi, G.A., 2011. Observational evidence for oceanic controls on hurricane intensity. J. Clim. 24, 1138–1153.
Mei, W., Pasquero, C., Primeau, F., 2012. The effect of translation speed upon the intensity of tropical cyclones over the tropical ocean. Geophys. Res. Lett. 39, L07801. http://dx.doi.org/10.1029/2011GL050765.
Mei, W., Xie, S.-P., Primeau, F., McWilliams, J.C., Pasquero, C., 2015. Northwestern Pacific typhoon intensity controlled by changes in ocean temperatures. Sci. Adv. 1, e1500014. http://dx.doi.org/10.1126/sciadv.1500014.
Menkes, C.E., Lengaigne, M., Marchesiello, P., Jourdain, N.C., Vincent, E.M., Lefevre, J., Chauvin, F., Royer, J.F., 2012. Comparison of tropical cyclogenesis indices on seasonal to interannual time- scales. Clim. Dyn. 38 (1–2), 301–321.
Niiler, P.P., Sybrandy, A.S., Bi, K., Poulain, P.M., Bitterman, D., 1995. Measurements of the water-following capability of holey-sock and TRISTAR drifters. Deep-Sea Res. 1, 1951–1964.
Niiler, P.P., 2001. The World Ocean Surface Circulation. In: Siedler, G., Church, J., Gould, J. (Eds.), Ocean Circulation and Climate: Observing and Modeling the Global OceanInt. Geophys. Ser. Vol. 77. Academic Press, pp. 193–204.
Pazan, S.E., Niiler, P.P., 2001. Recovery of near-surface velocity from undrogued drifters. J. Atmos. Ocean. Technol. 18, 476–489.
Price, J.F., 1981. Upper ocean response to a hurricane. J. Phys. Oceanogr. 11, 153–175.
Price, J.F., 1983. Internal wave wake of a moving storm. Part I: scales, energy budget and observations. J. Phys. Oceanogr. 13, 949–965.
Price, J.F., Sanford, T.B., Forristall, G.Z., 1994. Forced stage response to a moving hurricane. J. Phys. Oceanogr. 24, 233–260.
Sanford, T.B., Price, J.F., Girton, J.B., 2011. Upper-ocean response to hurricane Frances (2004) observed by profiling EM-APEX floats. J. Phys. Oceanogr. 41, 1041–1056.
Steele, J., Thorpe, S., Turekian, K., 2009. Elements of Physical Oceanography. second ed. Elsevier Ltd.
Sullivan, P.P., Romero, L., McWilliams, J.C., Melville, W.K., 2012. Transient evolution of Langmuir turbulence in ocean boundary layers driven by hurricane winds and waves. J. Phys. Oceanogr. 42, 1959–1980.
Teague, W.J., Jarosz, E., Wang, D.W., Mitchell, D.A., 2007. Observed oceanic response over the upper continental slope and outer shelf during hurricane Ivan. J. Phys. Oceanogr. 37, 2181–2206.